Charge Transport through Ferrocene 1,1′-Diamine Single-Molecule Junctions

*Karthiga Kanthasamy, Markus Ring, Dennes Nettelroth, Christoph Tegenkamp, Holger Butenschön, Fabian Pauly, and Herbert Pfnür**

The charge transport through ferrocene 1,1′-diamine (FDA) molecules between gold electrodes is investigated using the mechanically controllable break junction technique combined with a theoretical framework of density functional theory simulations to understand the physics of these molecular junctions. The characteristic conductances of the molecule are measured at low bias as well as current–voltage (IV) characteristics. By fitting the IV characteristics to the single-level model, the values for the position of the molecular level, mainly responsible for the transport, and its coupling to the leads, are obtained. The influence of the binding sites, molecular conformation, and electrode distance are systematically studied from a theoretical perspective. While a strong dependence of conductance on the adsorption geometry is found, the decrease of conductance as a function of electrode distance arises mainly from a decrease of coupling strength of the molecular electronic orbitals through a reduced overlap and, to a lesser extent, from a shift of their alignment with respect to the Fermi energy.

1. Introduction

Research in the field of molecular electronics aims at exploring the limits of miniaturization of electronic components in future nanoelectronic devices. Numerous studies on single-molecule junctions in the direction of electrical,[1,2] chemical,[3] mechanical,[4,5] thermal,[6] and optical[7,8] properties have been carried out in the past two decades with a variety of molecules and contact electrodes after a revolutionary suggestion by Aviram and Ratner[9] to exploit inherent properties of molecules in electrical circuits. The electronic transport through molecular junctions depends on the coupling of the frontier molecular orbitals to the metallic electrodes and the relative alignment of the molecular energy levels to the Fermi energy of the electrodes.[10,11] Both theoretical and experimental studies address different aspects, such as the influence on charge transport due to variations of molecular length, of end groups, contact electrodes, or temperature.[6,12–21] In order to exploit molecules in electric circuits, their physical, chemical, and electrical properties must be well known, when they are in contact to the electrodes. Examples of recent characterizations of single molecules between metallic contacts comprise alkanes,[13,22,23] p-conjugated,[2,24–30] and metal-organic[31,32] molecules as backbones for further studies. Among the metal-organic molecules, ferrocene $(C_5H_5)_2Fe$ as a functional unit has long been suggested as an attractive candidate,[33–35] as it is chemically very stable and rotationally flexible: The two cyclopentadienyl (Cp) rings bound to a central Fe atom can be rotated against

K. Kanthasamy, Prof. C. Tegenkamp, Prof. H. Pfnür
Institut für Festkörperphysik
ATMOS
Appelstr. 2, D-30167 Hannover, Germany
E-mail: pfnuer@fkp.uni-hannover.de
M. Ring, Prof. F. Pauly
Fachbereich Physik
Universitätsstr. 10, D-78464 Konstanz, Germany
D. Nettelroth, Prof. H. Butenschön
Institut für Organische Chemie
Leibniz Universität Hannover
Schneiderberg 1B, D-30167 Hannover, Germany
Prof. C. Tegenkamp, Prof. H. Pfnür
Laboratorium für Nano- und Quantenengineering
Schneiderberg 30, D-30167 Hannover, Germany

DOI: 10.1002/smll.201601051

each other without significant activation which results in stressless adsorption between contacts.[36] A molecular wire, containing ferrocene as the central functional molecular unit, has been reported to exhibit remarkably high conductance in comparison to an organic wire of similar length without ferrocene unit.[37] Most recent research with ferrocene as functional unit has been done with thiols as end groups and noble metals as electrode materials, such as Ag[36,38–40] or Au.[41,42] The Au-thiol bond is known to be strong and very robust,[18,43,44] and several experiments have been carried out with this combination.[17,19,45,46] On the other hand, the strong bond also leads to electrode deformation while stretching the gold electrode.[19,43] Therefore, weaker bonding through amine is an alternative, which has successfully been used in both theoretical and experimental studies,[47–49] and has been observed to lead to a well-defined molecular conductance.[50–52] Amines form a stable bond between low-coordinated Au atoms of the electrode and the p-conjugated molecular backbone.[48,49] Therefore, the combination of ferrocene as molecular unit and amine as linker group constitutes an interesting system for molecular transport.

This motivated us to study the electronic properties of FDA using the mechanically controllable break junction (MCBJ) technique with Au as contact electrode. We investigated the nature of the molecular conduction by varying the distance between the electrodes and systematically explored the influence mainly of stretching on the molecular junction conductance. Detailed insight at the atomistic scale, such as selection of favorable adsorption sites and energy level alignments, cannot be directly extracted from the available experimental techniques to date. For interpreting the experimental results, they are complemented by theoretical computations of quantum transport in the framework of density functional theory (DFT) and the non-equilibrium Green's function formalism.

2. Experimental Results

2.1. Molecular Conductance Measurements

The experiments were performed with an MCBJ setup using lithographic gold electrodes to contact the molecules (see Experimental Section). The characteristic conductance of the gold junctions with molecules was measured at a small constant bias voltage of 1 mV, while opening and closing them by pushing or withdrawing a rod at a fixed speed from underneath the MCBJ geometry. The main advantages of this setup are the robust nature and the controlled stability at the atomic scale.[53] The conductance changes in a stepwise manner as a function of electrode separation due to the reduction of the cross section of atomic gold wires. They ultimately break when the wires are only one atom wide.[54,55] In the presence of molecules, additional steps below $1G_0 = 2e^2/h$ are observed due to adsorption of one or several molecules, bridging the gap between the electrodes.

Figure 1a shows conductance–distance traces for three different opening cycles in the presence of molecules. These graphs were obtained after having performed several opening

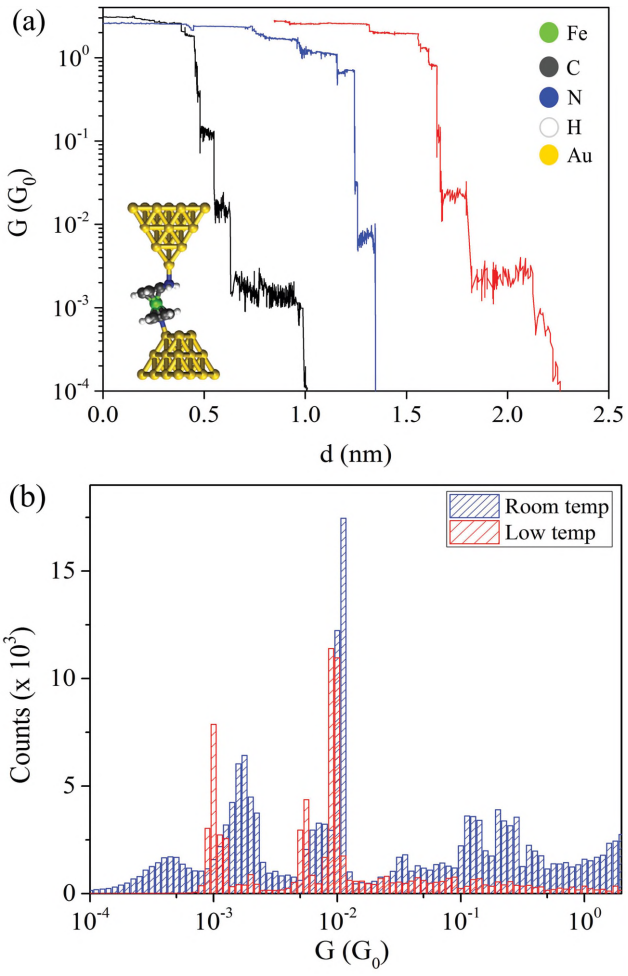

Figure 1. a) Stepwise change of conductance, G, at room temperature as a function of electrode separation, d, obtained by pulling the electrodes apart in the presence of FDA. Different conductance–displacement traces are offset along the displacement axis for clarity. A possible junction geometry with an FDA molecule between gold contacts is displayed as an inset. b) Conductance histograms obtained from 250 opening and closing traces at $T = 300$ and 120 K, respectively, with a bin size of $\Delta\log(G/G_0) = 0.05$. They were recorded at a bias voltage at 1 mV.

and closing cycles, starting at a maximum conductance between 2 and 3 G_0. Only those opening and closing traces have been included in the histogram (Figure 1b) that exhibit plateaus in the conductance range below 0.5 G_0, characteristic of molecular conductance. The initially constant conductance in Figure 1a is due to mechanical hysteresis of the break junction setup. Therefore, these data were not included in Figure 1b. Close to 1 G_0 several small steps are seen frequently in those curves that reflect the interaction of metal and molecule(s) squeezed between the contacts. Below $1G_0$, a maximum displacement of 9 Å of the electrodes was possible before the contact was lost. The DFT calculations yield an N–N distance of 6.5 Å for the isolated FDA molecule, which is somewhat shorter than the maximum displacement observed.

In other words, both compressing and/or stretching of molecular bonds, together with relaxation of the Au electrodes are required to observe a molecular conductance over this wide range of electrode distance variations. Since

opening and closing cycles are not the same in terms of conductance values and lengths of the plateaus due to different breaking geometries and molecular configurations relative to the electrodes, a histogram is plotted to learn more about the characteristic conductance at the molecular level. We have performed our measurements at room temperature (T = 300 K) and with cooling by liquid nitrogen (lN$_2$) (T = 120 K).

Generally, the peak positions in the histograms correspond to frequently occurring junction configurations, exhibiting the highest stability of the molecules between the contacts. They can be viewed as averages over molecular geometry and adsorption sites. These highly stable configurations seem to be more concentrated at specific values of conductance at low temperature compared to room temperature. While the maxima close to 0.01 G_0 and around 6×10^{-3} G_0 appear in both histograms (see Figure 1b), the further dominant peak at 1×10^{-3} G_0 at low temperature seems to be split into two peaks around 4×10^{-4} G_0, and at 1.5×10^{-3} G_0 for the room temperature measurements. Although no definite solution can be given based on these results, this finding can be rationalized by the reduced mobility of Au atoms at low temperature so that the contact atoms cannot fully relax at a given average contact separation on presence of the bonding molecule. As concluded from calculations (see below), this range of conductance corresponds to an already slightly stretched molecule. Since conductance depends on the local binding geometry, as corroborated by theory, this explanation is plausible.

The differences between low- and high-temperature conductance in the range above 0.1 G_0 may have a similar origin. The histograms in this conductance range exhibit two small maxima at 0.13 and 0.25 G_0, which are less pronounced at low temperature, and the overall probability to observe values in this range is higher at room temperature. Although we cannot exclude contributions from more than one molecule in this range, the appearance of clear maxima can be taken as indication for a high conductance of single molecules. Such high conductances were recently reported for similarly short benzene-dithiol molecules through shot noise measurements.[30] This interpretation implies that temperature has no dominant influence on molecular conductance at high conductance for this molecule,[56] as expected for coherent transport.

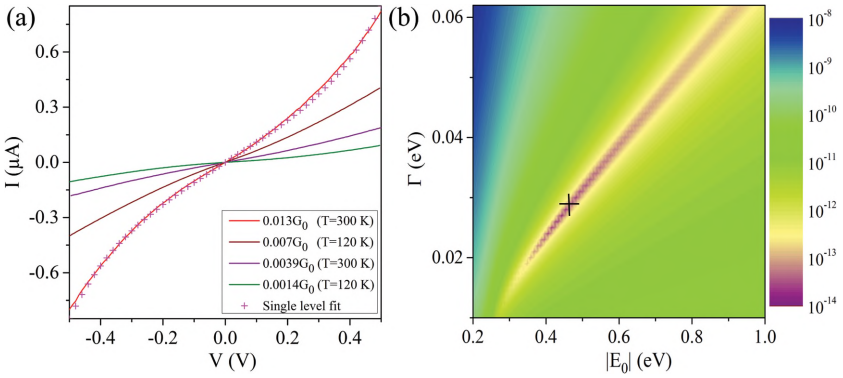

Figure 2. a) Current I versus voltage V plots at room and lN$_2$ temperatures. Also a single-level fit for the curve at 0.013 G_0 with $|E_0| = 0.46$ eV and $\Gamma = 27$ meV is indicated. b) 2D contour plot of the error of the single-level model fit to the experimental IV curve as a function of coupling and energy level position for the experimental curve with 0.013 G_0. The best-fit parameters are marked by the cross.

2.2. Current–Voltage Measurements

Taking advantage of the high mechanical stability of the MCBJ setup, IV measurements are performed in order to get a deeper understanding of the electrical properties of FDA. To perform such measurements, the junction was opened using the piezo motor at a constant speed of 15 pm s^{-1}. If the conductance remained constant below 1 G_0 for a few picometer of electrode displacements at room and at lN$_2$ temperatures, we stopped the motor at such a position and observed the conductance value over time. If the conductance turned out to be stable over several minutes, IV measurements were performed by ramping the voltage from +0.5 to –0.5 V. This range is limited by electrical breakdown of the covalently bonded Au–FDA–Au molecular junctions,[57] which leads to instabilities and irreversible changes of the molecular contact at higher electric fields. The conductance value G at zero bias is taken as reference for each IV curve. These IV measurements were repeated for other distances between the electrodes. Sometimes, it was necessary to re-establish contact between the metallic electrodes, before the experiment could be repeated. Typically, 30 measurements were taken at every distance, i.e., for every stable junction realization. The graphs in **Figure 2**a show the average of the IV measurements at selected electrode positions at room temperature and at lN$_2$ temperature.

Interestingly, the first-order derivatives (not shown) of the IV curves show only a continuous variation of slopes, but no characteristic peaks or steps. This is in contrast to the results obtained with ferrocene dithiol,[37,40] where peaks were found with silver contacts.[40] We see, however, a significant variation in the IV curves as a function of their zero-bias conductance.

In order to understand this more quantitatively, we tentatively assume that electronic transport is dominated by a single molecular level, and fit the IV curves by the single-level model.[58–60] According to this model, the current through the molecular junction is governed by the formula

$$I(V) = \frac{2e}{h} \int T(E,V)\left[f\left(E + \frac{eV}{2}\right) - f\left(E - \frac{eV}{2}\right)\right] dE \qquad (1)$$

with the transmission function given by Breit–Wigner formula

$$T(E,V) = \frac{4\Gamma_l \Gamma_r}{\left[E - E_0(V)\right]^2 + \left[\Gamma_l + \Gamma_r\right]^2}. \qquad (2)$$

Here, E_0 is the position of the molecular energy level with respect to the Fermi energy of the metal, E_F, that we set to

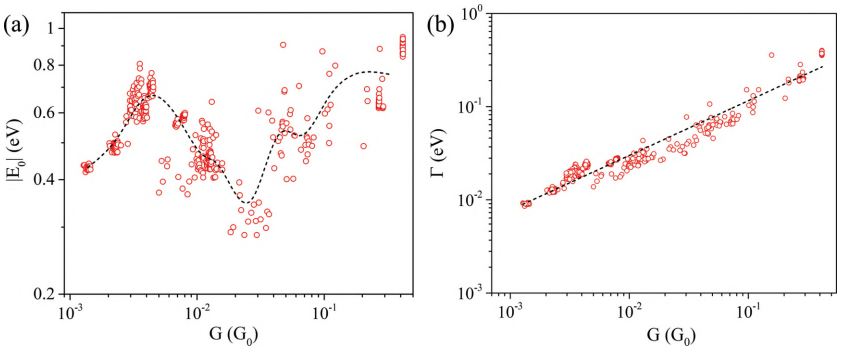

Figure 3. a) Energy level $|E_0|$ and b) coupling Γ, as extracted from the best fits of the single-level model to experimental *IV* curves as a function of zero-bias conductance. The panels contain all the measured *IV* curves at $T = 300$ and 120 K. The black dashed line for E_0 shows a spline interpolation between averages taken with a bin size of $\Delta \log(G/G_0) = 0.2$. For Γ, it represents a power-law function ($\Gamma = ag^b$) that is fitted to the experimental data with $g = G/G_0$, $a = 0.4 \pm 0.03$ eV, and $b = 0.5$.

zero, f is the Fermi-Dirac distribution, and $\Gamma_L = \Gamma_R$ are the effective electronic couplings to the left and right electrodes, respectively. Since we find in the experiment mostly symmetric *IV* characteristics, we assume the coupling parameters to be equal in the following, i.e., $\Gamma = \Gamma_L = \Gamma_R$, and E_0 to be voltage independent. Since only the absolute value of E_0 can be determined through conductance measurements, we will refer to $|E_0|$ in the following.

As an example, Figure 2a shows the best fit of the experimental curve at $G = 0.013\ G_0$, using Equations (1) and (2) with $|E_0| = 0.46$ eV and $\Gamma = 27$ meV. The statistical error of the fit, determined as the sum of mean square deviations between the fit and the original data, is shown in Figure 2b as a 2D contour plot. The global minimum is indicated by a cross. The uncertainty in $|E_0|$ is estimated from the 95% confidence level (2σ deviation) to be ±0.01 eV in this case, that of Γ amounts to ±1 meV. As it is apparent from Figure 2b, Γ and $|E_0|$ are coupled to some extent, but not fully. These single-level fits were repeated for all measured *IV* curves, and the level alignments and coupling constants were extracted, as shown in **Figure 3**.

As seen from Figure 3a, the scatter in $|E_0|$ for different measurements at the same G is significantly larger than the uncertainties of the fits. An obvious explanation is that different configurations with different effective level alignments lead to the same conductance at small voltages. Moreover, $|E_0|$ varies systematically as a function of conductance. Starting at around 0.4 eV at $G = 0.001\ G_0$, it goes through a maximum of 0.7 eV at $G = 0.004\ G_0$, decreases to values around 0.3 eV at a conductance of $G = 0.02\ G_0$, before it rises again above $G = 0.05\ G_0$. The coupling constant turns out to be only weakly coupled to this variation of $|E_0|$. It increases rather monotonously as a function of conductance over the whole measurement range from 0.001 to 0.4 G_0. Setting $g = G/G_0$, a power law of $\Gamma = ag^b$ was fitted to the experimental data in Figure 3b with $a = 0.4 \pm 0.04$ eV and $b = 0.5$. This is justified by Equation (2), since the (low-temperature) conductance $G \approx G_0 T(E_F, 0)$ should be proportional to Γ^2, if E_0 is constant and large in comparison to Γ. In summary, the energy level $|E_0|$ varies by a factor of two with conductance, while the coupling Γ increases monotonically and follows the expected square-root dependence on the conductance. This leads to the conclusion that for the strongly off-resonant situation, present for FDA, the coupling is the determining factor for the variation of the zero-bias conductance.

2.3. Theoretical Results and Discussion

To understand the experimental findings in terms of a microscopic picture, we performed DFT calculations of an FDA molecule between gold contacts with the program package TURBOMOLE.[61] Quantum transport data were calculated from the DFT Hamiltonian.[62]

In order to explore the dependence of the transmission on configuration, we analyzed several junction geometries as a function of distance between the electrodes. We chose the amine side groups of FDA to be either opposite to each other (point symmetric with respect to Fe, referred to as "1") or we rotated one of the cyclopentadienyl rings by 36° (rotated or "2"). Both conformations of the isolated molecule are energetically similar with less than 1 meV difference in total energy, while all other rotation angles lead to energetically higher states. For each of these conformations, three contact structures were constructed from sharp and blunt tips: sharp–sharp (ss), blunt–sharp (bs), and blunt–blunt (bb). These Au tips on each side of the molecular junction are oriented with their [111] directions along the transport (or z) direction. They consist of 20 or 19 Au atoms, respectively. The sharp tip ends with a single atom, whereas for the blunt one this last atom was removed. The three contact geometries with two different FDA configurations produce six different types of geometries in total: ss1, ss2, bs1, bs2, bb1, and bb2. For their construction, we place the tips directly opposite to each other and put the second tip at a similar z-distance from the molecule as the first trial position, after having relaxed the molecule on top of a single tip. Optimizing the geometry of the molecule inside the junctions, we find that the contacting amine group will bind directly to a single gold atom in all of these starting configurations. In order to change the separation between the electrodes, the distance between the two fixed outermost bulk layers of the pyramids was increased and decreased by ±0.1, ±0.25, ±0.5, and ±1 Å, and the contact was relaxed again to a local energetic minimum. Finally, the energy-dependent transmissions were calculated for the nine distances per type of configuration, yielding 54 Au-FDA-Au transmission curves.

The geometry of the bs1 junction is illustrated in **Figure 4**a, and examples of zero-bias transmission curves $T(E, V = 0)$ for this configuration are shown in Figure 4b. Their behavior close to the Fermi energy indicates off-resonant transport. For the selected curves, the transmission is dominated by the frontier orbitals, i.e., the highest occupied molecular orbital (HOMO) at –0.8 to –0.6 eV and the lowest unoccupied molecular orbital (LUMO) at 2.1–2.3 eV. For further junction geometries and

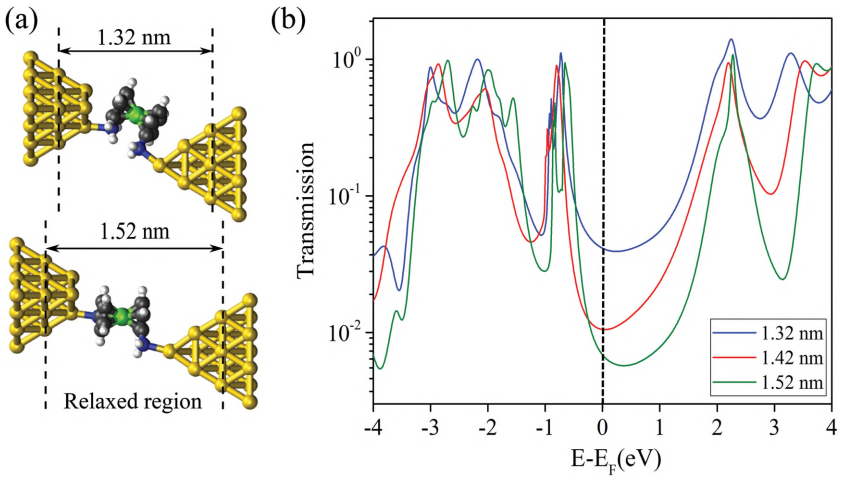

Figure 4. a) Sample junction geometries for bs1. b) Transmissions for the bs1 type of junctions for various electrode separations.

transmission curves used in our analysis, we refer the reader to the Supporting information.

Direct analysis of the transmission curves *T (E, V = 0)*, see, e.g., Figure 4b, indicates that the HOMO of FDA is typically closer to the Fermi energy than the LUMO. Since, however, the broadening of the HOMO is often less than that of the LUMO, the conductance, i.e., the transmission close to the Fermi energy, is often influenced by both frontier orbitals. Depending on the type of junction, there may also be other effects, stemming, e.g., from metal-like background tunneling for very short electrode separations to Fano-like anti-resonances. We discuss further the consequences of such limitations of the single-level model in the Supporting Information.

In order to make a close comparison with experiment for all these situations, we decided to integrate *T (E, V = 0)* according to Equation (1) to get simulated *IV* curves. These were then fitted with the single-level model in the same way as the experimental data in order to get comparable values for E_0 and Γ. The obtained results are shown in **Figure 5** together with the averages of the experimental data from Figure 3.

We find computed single-molecule conductances to be compatible with the range of experimentally measured "molecular" values from around 10^{-3} G_0 to 10^{-1} G_0. For a fixed conductance G, overall theory values for the effective energy level, E_0, tend to be overestimated. In order to yield the same conductance value, the computed effective coupling parameter, Γ, must consequently be too large as well, based on the relations $G = G_0T$ (E_F, $V = 0$) and Equation (2). Both in simulation and experiment an increasing conductance is connected with an increase in electronic broadening, which to first approximation follows the square-root dependence described above. Furthermore, the DFT simulations show a clear sensitivity of conductance to the binding configurations. It is important to mention, however, that although the same G can be obtained with several different contact geometries, these differ in part significantly in the effective values of E_0 and Γ and can thus be discriminated. This variability of E_0 and Γ with configuration at fixed G explains qualitatively the experimentally observed scatter in the data seen in Figure 3, which also appears, although differently, in Figure 5 for the selected geometries simulated here.

On the other hand, the experimental variation of E_0 in Figure 3a is much smaller than the span of E_0 obtained in the simulations for the various types of contact geometries for a particular value of G in Figure 5a. From this observation we conclude that the preference for certain contact configurations varies as a function of contact separation.

Interestingly, even when taking this scatter in the experimental data into account, they follow an S-shaped dependence of E_0 as a function of G, but no single tested combination of contact geometries yields a qualitatively similar dependence in the simulations. As an example, conformation bb2 shows essentially no dependence of E_0 on G, contrary to experiment. Therefore, this configuration is most likely not realized experimentally. For low G (between 10^{-2} G_0 and 10^{-3} G_0), i.e., for the largest measurable separations between the contacts, we find that the models with single atoms at the end (sharp tips, ss1 and ss2) describe the experimental values for E_0 as a function of G best. This corroborates the intuitive picture that for large contact separations contact configurations ending with single metal atoms are favored. This situation seems to change for G between 10^{-2} G_0 and 10^{-1} G_0, where a significant decrease of E_0 is found. Remarkably, basically only configuration bb1 (blunt tips, non-rotated molecular rings) reproduces qualitatively this decrease of E_0, while it yields much higher values of E_0 than experimentally observed at G below 10^{-2} G_0. At these intermediate contact separations, other configurations than those ending with single atoms become important. Since the molecular level alignment E_0 depends strongly on the internal molecular degrees of freedom, the non-rotated conformation appears to be favored.

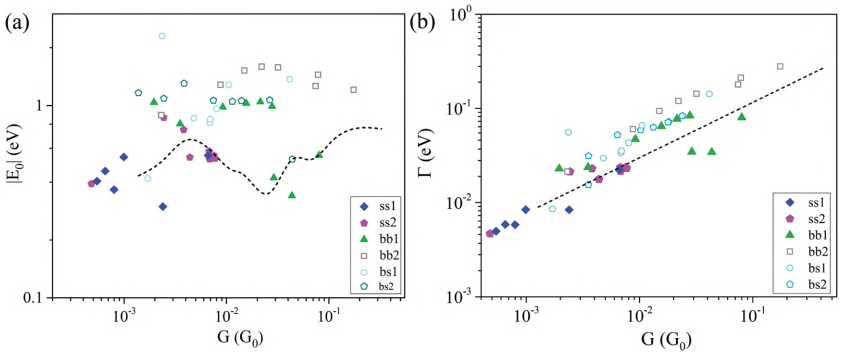

Figure 5. a) Energy level $|E_0|$ and b) coupling Γ as a function of zero-bias conductance G, as extracted from best fits of the single-level model to theoretically determined *IV* curves. The dashed lines in both figures show the experimental trends and are the same as in Figure 3.

For G above 0.1 G_0, where again an increase of E_0 is observed experimentally, the situation gets more complicated, since direct tunneling between the metal electrodes may add to the molecular conductance channel. Therefore, the general physical situation is less clear than at lower conductance. Also junction geometries with more extended Au surfaces than those used here should be tested in order to get a more realistic picture at these close electrode separations. Because of the complexity of this problem, this goes far beyond the scope of this paper.

The experimentally extracted coupling between electrodes and molecules and the concomitant broadening of molecular levels, here expressed by just the effective broadening of a single resonance, follows nicely the overall trend described by a square-root dependence on G, as we discussed in context with Figure 2b. This general trend is well reproduced by the DFT simulations in Figure 5b. Conformation-specific differences between experimental and simulated values follow the same tendencies as described above for E_0, and shall not be repeated here. This demonstrates the close relationship between Γ and E_0.

Generally charge transport through the molecule is small for the largest part of the junction types tested here, which could lead to electrons trapped on the molecule for some time. However, there are no indications of Coulomb blockade effects in our experimental *IV* curves. Instead, it seems that direct coupling of HOMO and LUMO states with the orbitals of the electrode and their modification by the chemical bonds determine the transmission through the FDA molecule. As corroborated by our theoretical simulations, this coupling can be controlled mechanically. It is continuously modified by stretching or compressing the molecular junctions and alters the transmission mostly through this quantum mechanical entity.

Our interpretations above are based on the assumption that single FDA molecules are present in the junctions. For benzene-dithiol, it has been shown recently through simultaneous studies of conductance and shot noise that conductance values between 10^{-2} G_0 and 0.24 G_0 are all due to a single conduction channel, and consequently single-molecule junctions.[30] While there are theoretical uncertainties due to the typical overestimation of conductance values in DFT calculations,[48] FDA is a similarly short molecule as benzene-dithiol, suggesting that it may serve as a similar broad-range, single-channel conductor. As shown in the Supporting Information, we also considered the situation of n parallel molecules. For this purpose, we extracted the behavior of the single-level model parameters, if the total, fitted *IV* characteristic arises from n molecules with identical *IV* curves that originate from the single-level model. In the off-resonant situation, we find that the effective level alignment stays rather constant with increasing n, or equivalently with increasing conductance, while $\Gamma \propto G^{1/2}$. This behavior is still compatible with the general situation described above both in theory and experiment, even if the experimental S-shaped behavior of E_0 is not reproduced. Ultimately, additional measurements are needed to discriminate between single- and multi-molecule junctions.

3. Summary and Conclusions

We have experimentally investigated the electrical transport through FDA molecules between gold contacts by stretching and compressing the molecular junctions. These measurements were complemented by ab-initio simulations of quantum transport with several different molecule and electrode configurations, chosen to test the electronic transmission properties of a variety of likely junction geometries.

Although from the comparison of experiment with theory we do not expect quantitative agreement, the results yield a picture of the mechanism of electronic transport and qualitatively agree regarding trends of the conductance behavior. We find considerable sensitivity of conductance on the adsorption geometry at the contacts and, under the assumption that single-molecule junctions are realized, conclude that specific contact configurations are favored depending on contact distance. These specific configurations can also explain the oscillating position of the effective single level as a function of zero-bias conductance. For the overall behavior, the fit of the data to the single-level model allows the interpretation that the decrease of conductance as a function of electrode distance arises mainly from a decrease in coupling strength of the molecular electronic orbitals through a reduced overlap and to a lesser extent from a shift of their alignment with respect to the Fermi energy. Due to this mechanism, charge transport through FDA can be tuned by stretching, compressing, or rotating the cyclopentadienyl rings with respect to each other.

4. Experimental Section

The gold break junctions were fabricated on a steel substrate coated with an insulating polyimide by the electron beam lithography technique. Gold (100 nm thick) electrodes were deposited by thermal evaporation. Detailed information about the sample fabrication can be found elsewhere.[63] The gold electrodes were mounted on a three-point home-made setup. FDA at a concentration of 1 mmol and dissolved in toluene was added dropwise to the junction and allowed to dry for a few seconds. The molecules were synthesized according to the procedure of Shafir et al.[64] The adsorption of the molecule on the surface without defragmentation was confirmed by X-ray photoelectron spectroscopy measurements (see the Supporting Information). Later the sample was transferred to the measurement chamber, which was pumped to 10^{-7} mbar. The measurement chamber was designed for measurements at room temperature and at liquid N_2 temperature.

Data Acquisition: The free-standing gold junction at the center was strained using a piezo motor from below the sample. As the strain increases, the junctions narrows, leading to a stepwise change in the conductance, which was measured by a Keithley 2401 source meter. The position of the motor and the conductance measurements were controlled by a LabVIEW program. Two types of measurements were done to study the molecular properties. First, the conductance measurements were carried out by repeatedly opening and closing junctions at a fixed voltage to get an approximate range of the molecular conductance values and peak widths in conductance histograms. Second, the junction was

opened slowly at constant motor speed, and at certain stable positions *IV* measurements were carried out by ramping the voltage from +0.5 to –0.5 V or vice versa in steps of 10 mV, and a minimum of 30 voltage sweeps were recorded at the fixed distance. The junction was again closed and opened, so that a new molecular junction was formed, and *IV* measurements were repeated at a different distance between the electrodes.

Supporting Information

Supporting Information is available from the Wiley Online Library or from the author.

Acknowledgements

The authors thank Detlef Zech (MBE) for gold deposition and Oliver Kerker (LNQE) for technical assistance in the clean room at Leibniz Universität Hannover. Furthermore, the authors acknowledge stimulating discussions with Marius Bürkle as well as technical assistance. M.R. and F.P. were supported through the German Research Foundation (DFG) and the Carl-Zeiss Foundation, respectively. The authors also thank the bwHPC initiative and the bwHPC-C5 project for providing the computational resources bwUniCluster and the JUSTUS HPC facility, on which part of this work was carried.

[1] E. Lörtscher, B. Gotsmann, Y. Lee, L. Yu, C. Rettner, H. Riel, *ACS Nano* **2012**, *6*, 4931.
[2] T. Kim, P. Darancet, J. R. Widawsky, M. Kotiuga, S. Y. Quek, J. B. Neaton, L. Venkataraman, *Nano Lett.* **2014**, *14*, 794.
[3] N. Darwish, I. Díez-Perez, S. Guo, N. Tao, J. J. Gooding, M. N. Paddon-Row, *J. Phys. Chem. C* **2012**, *116*, 21093.
[4] B. Q. Xu, X. Y. Xiao, N. J. J. Tao, *Am. Chem. Soc.* **2003**, *125*, 16164.
[5] M. Frei, S. V. Aradhya, M. Koentopp, M. S. Hybertsen, L. Venkataraman, *Nano Lett.* **2011**, *11*, 1518.
[6] J. Balachandran, P. Reddy, D. B. Dunietz, V. J. Gavini, *Phys. Chem. Lett.* **2012**, *3*, 1962.
[7] B. M. Briechle, Y. Kim, P. Ehrenreich, A. Erbe, D. Sysoiev, T. Huhn, U. Groth, E. Scheer Beilstein, *J. Nanotechnol.* **2012**, *3*, 798.
[8] M. Vadai, N. Nachman, M. Ben-Zion, M. Bürkle, F. Pauly, J. C. Cuevas, Y. J. Selzer, *Phys. Chem. Lett.* **2013**, *4*, 2811.
[9] A. Aviram, M. A. Ratner, *Chem. Phys. Lett.* **1974**, *29*, 277.
[10] R. Stadler, K. W. Jacobsen, *Phys. Rev. B* **2006**, *74*, 161405.
[11] H. Ishii, K. Sugiyama, E. Ito, K. Seki, *Adv. Mater.* **1999**, *11*, 605.
[12] Y. S. Park, A. C. Whalley, M. Kamenetska, M. L. Steigerwald, M. S. Hybertsen, C. Nuckolls, L. J. Venkataraman, *Am. Chem. Soc.* **2007**, *129*, 15768.
[13] F. Chen, X. Li, J. Hihath, Z. Huang, N. J. Tao, *Am. Chem. Soc.* **2006**, *128*, 15874.
[14] C. M. Kim, J. J. Bechhoefer, *Chem. Phys.* **2013**, *138*, 014707.
[15] P. Moreno-García, M. Gulcur, D. Z. Manrique, T. Pope, W. Hong, V. Kaliginedi, C. Huang, A. S. Batsanov, M. R. Bryce, C. Lambert, T. J. Wandlowski, *Am. Chem. Soc.* **2013**, *33*, 12228.
[16] C. A. Martin, D. Ding, H. S. J. van der Zant, J. M. van Ruitenbeek, *New J. Phys.* **2008**, *10*, 065008.
[17] K. H. Müller, *Phys. Rev. B* **2006**, *73*, 045403.
[18] E. Lörtscher, C. J. Cho, M. Mayor, M. Tschudy, C. Rettner, H. Riel, *ChemPhysChem* **2011**, *12*, 1677.
[19] Y. Kim, T. J. Hellmuth, M. Bürkle, F. Pauly, E. Scheer, *ACS Nano* **2011**, *5*, 4104.
[20] W. Hong, D. Z. Manrique, P. Moreno-García, M. Gulcur, A. Mishchenko, C. J. Lambert, M. R. Bryce, T. J. Wandlowski, *Am. Chem. Soc.* **2012**, *134*, 2292.
[21] V. B. Engelkes, J. M. Beebe, C. D. J. Frisbie, *Am. Chem. Soc.* **2004**, *126*, 14287.
[22] C. C. Kaun, T. Seideman, *Phys. Rev. B* **2008**, *77*, 033414.
[23] J. M. Beebe, B. S. Kim, J. W. Gadzuk, C. Daniel Frisbie, J. G. Kushmerick, *Phys. Rev. Lett.* **2006**, *97*, 026801.
[24] M. Bürkle, J. K. Viljas, D. Vonlanthen, A. Mishchenko, G. Schön, M. Mayor, T. Wandlowski, F. Pauly, *Phys. Rev. B* **2012**, *85*, 075417.
[25] A. Mishchenko, L. A. Zotti, D. Vonlanthen, M. Bürkle, F. Pauly, J. C. Cuevas, M. Mayor, T. J. Wandlowski, *Am. Chem. Soc.* **2011**, *133*, 184.
[26] A. Mishchenko, D. Vonlanthen, V. Meded, M. Bürkle, C. Li, I. V. Pobelov, A. Bagrets, J. K. Viljas, F. Pauly, F. Evers, M. Mayor, T. Wandlowski, *Nano Lett.* **2010**, *10*, 156.
[27] C. Li, I. Pobelov, T. Wandlowski, A. Bagrets, A. Arnold, F. Evers, *J. Am. Chem. Soc.* **2008**, *130*, 318.
[28] M. Kamenetska, M. Koentopp, A. C. Whalley, Y. S. Park, M. L. Steigerwald, C. Nuckolls, M. S. Hybertsen, L. Venkataraman, *Phys. Rev. Lett.* **2009**, *102*, 126803.
[29] J. Reichert, R. Ochs, D. Beckmann, H. B. Weber, M. Mayor, H. V. Löhneysen, *Phys. Rev. Lett.* **2002**, *88*, 176804.
[30] M. A. Karimi, S. G. Bahoosh, M. Herz, R. Hayakawa, F. Pauly, E. Scheer, *Nano Lett.* **2016**, *16*, 1803.
[31] R. Liu, S. H. Ke, W. Yang, H. U. J. Baranger, *Chem. Phys.* **2006**, *124*, 024718.
[32] Z.-F. Xu, Y. Xie, W.-L. Feng, H. F. J. Schaefer, *Phys. Chem. A* **2003**, *107*, 2716.
[33] J. J. Bishop, A. Davison, M. L. Katcher, D. W. Lichtenberg, R. E. Merrill, J. C. J. Smart, *Organomet. Chem.* **1971**, *27*, 241.
[34] C. A. Nijhuis, W. F. Reus, G. M. J. Whitesides, *Am. Chem. Soc.* **2010**, *132*, 18386.
[35] N. Nerngchamnong, L. Yuan, D.-C. Qi, J. Li, D. Thompson, C. A. Nijhuis, *Nat. Nanotechnol.* **2013**, *8*, 113.
[36] J. Meyer, T. Bredow, C. Tegenkamp, H. J. Pfnür, *Chem. Phys.* **2006**, *125*, 194705.
[37] S. A. Getty, C. Engtrakul, L. Wang, R. Liu, S. H. Ke, H. U. Baranger, W. Yang, M. S. Fuhrer, L. R. Sita, *Phys. Rev. B* **2005**, *71*, 241401.
[38] C. Tegenkamp, J. Schmeidel, H. Pfnür, *Surf. Sci.* **2011**, *605*, 267.
[39] T. Bredow, C. Tegenkamp, H. Pfnür, J. Meyer, V. V. Maslyuk, I. J. Mertig, *Chem. Phys.* **2008**, *128*, 064704.
[40] G. Gardinowski, J. Schmeidel, H. Pfnür, T. Block, C. Tegenkamp, *Appl. Phys. Lett.* **2006**, *89*, 063120.
[41] L. Müller-Meskamp, S. Karthäuser, R. Waser, M. Homberger, Y. Wang, U. Englert, U. Simon, *Surf. Sci.* **2009**, *603*, 716.
[42] T. Weidner, N. Ballav, M. Zharnikov, A. Priebe, N. J. Long, J. Maurer, R. Winter, A. Rothenberger, D. Fenske, D. Rother, C. Bruhn, H. Fink, U. Siemeling, *Chem. Eur. J.* **2008**, *14*, 4346.
[43] Z. Huang, F. Chen, P. A. Bennett, N. J. Tao, *Am. Chem. Soc.* **2007**, *129*, 13225.
[44] M. Tsutsui, M. Taniguchi, T. J. Kawai, *Am. Chem. Soc.* **2009**, *131*, 10552.
[45] X. Li, J. He, J. Hihath, B. Q. Xu, S. M. Lindsay, N. J. Tao, *Am. Chem. Soc* **2006**, *128*, 2135.
[46] D. Dulic´, F. Pump, S. Campidelli, P. Lavie, G. Cuniberti, A. Filoramo, *Angew. Chem., Int. Ed.* **2009**, *48*, 8273.
[47] P. Vélez, S. A. Dassie, E. P. M. Leiva, *Phys. Rev. B* **2010**, *81*, 235435.
[48] S. Y. Quek, L. Venkataraman, H. J. Choi, S. G. Louie, M. S. Hybertsen, J. B. Neaton, *Nano Lett.* **2007**, *7*, 3477.
[49] Z. Li, D. S. Kosov, *Phys. Rev. B* **2007**, *76*, 035415.

[50] M. S. Hybertsen, L. Venkataraman, J. E. Klare, A. C. Whalley, M. L. Steigerwald, C. J. Nuckolls, *Phys. Condens. Matter* **2008**, *37*, 374115.
[51] L. Venkataraman, J. E. Klare, I. W. Tam, C. Nuckolls, M. S. Hybertsen, M. L. Steigerwald, *Nano Lett.* **2006**, *6*, 458.
[52] L. Venkataraman, J. E. Klare, C. Nuckolls, M. S. Hybertsen, M. L. Steigerwald, *Nature* **2006**, *442*, 904.
[53] J. M. van Ruitenbeek, A. Alvarez, I. Piñeyro, C. Grahmann, P. Joyez, M. H. Devoret, D. Esteve, C. Urbina, *Rev. Sci. Instrum.* **1996**, *67*, 108.
[54] M. Dreher, F. Pauly, J. Heurich, J. C. Cuevas, E. Scheer, P. Nielaba, *Phys. Rev. B* **2005**, *72*, 075435.
[55] H. Ohnishi, Y. Kondo, K. Takayanagi, *Nature* **1998**, *395*, 780.
[56] Q. Lu, C. Yao, X. Wang, F. J. Wang, *Phys. Chem. C* **2012**, *116*, 17853.
[57] H. Li, T. A. Su, V. Zhang, M. L. Steigerwald, C. Nuckolls, L. J. Venkatraman, *Am. Chem. Soc.* **2015**, *137*, 5028.
[58] L. A. Zotti, T. Kirchner, J. C. Cuevas, F. Pauly, T. Huhn, E. Scheer, A. Erbe, *Small* **2010**, *6*, 1529.
[59] S Datta. *Electronic Transport in Mesoscopic Systems*, Cambridge University Press, UK **1997**.
[60] R. Frisenda, S. Tarkuç, E. Elena Galán, M. L. Perrin, R. Eelkema, F. C. Grozema, J. H. S. van der Zant, *Beilstein J. Nanotechnol.* **2015**, *6*, 1558.
[61] TURBOMOLE V6.5 **2010**, a development of University of Karlsruhe and Forschungszentrum Karlsruhe GmbH, 1989–2007, TURBOMOLE GmbH, since 2007, http://www.turbomole.com (accessed April 2013).
[62] F. Pauly, J. K. Viljas, U. Huniar, M. Häfner, S. Wohlthat, M. Bürkle, J. C. Cuevas, G. Schön, *New J. Phys.* **2008**, *10*, 125019.
[63] K. Kanthasamy, H. Pfnür, *Beilstein J. Nanotechnol.* **2015**, *6*, 1690.
[64] A. Shafir, M. P. Power, G. D. Whitener, J. Arnold, *Organometallics* **2000**, *19*, 3978.